
Article:
Du, H, Peacock, CL orcid.org/0000-0003-3754-9294, Chen, W et al. (1 more author) (2018) Binding of Cd by ferrihydrite organo-mineral composites: Implications for Cd mobility and fate in natural and contaminated environments. Chemosphere, 207. pp. 404-412. ISSN 0045-6535

https://doi.org/10.1016/j.chemosphere.2018.05.092

Binding of Cd by ferrihydrite organo-mineral composites: Implications for Cd mobility and fate in natural and contaminated environments

Huihui Du,[1, 2, 4] Caroline L. Peacock,[3, *] Wenli Chen,[1] Qiaoyun Huang[1, 2, *]

[1] State Key Laboratory of Agricultural Microbiology, College of Resources and Environment, Huazhong Agricultural University, Wuhan 430070, PR China

[2] Hubei Key Laboratory of Soil Environment and Pollution Remediation, College of Resources and Environment, Huazhong Agricultural University, Wuhan 430070, China

[3] University of Leeds, School of Earth and Environment, Leeds LS2 9JT, UK

[4] College of Resources and Environment, Hunan Agricultural University, Changsha 410128, PR China

*Corresponding Author: Qiaoyun Huang and Caroline L. Peacock

Email: qyhuang@mail.hzau.edu.cn; C.L.Peacock@leeds.ac.uk

ABSTRACT

Adsorption and coprecipitation of organic matter with iron (hydr)oxides can alter iron (hydr)oxide surface properties and their reactivity towards nutrient elements and heavy metals. Organo−mineral composites were synthesized using humic acid (HA) and iron oxide, during coprecipitation with ferrihydrite (Fh) and adsorption to pre-formed Fh with two C loadings. The Fh−HA coprecipitated composites have a higher C content and smaller surface area compared to the equivalent adsorbed composites. NanoSIMS shows there is a high degree of spatial correlation between Fe and C for both composites, but C distribution is more uniform in the coprecipitated composites. The C 1s NEXAFS reveals a similar C composition between the Fh−HA coprecipitated and adsorbed composites. However composites at high carbon loading are more enriched in aromatic C, likely due to preferential binding of carboxyl functional groups on aromatic rings in the HA. The amount of Cd sorbed is independent of the composite type, either coprecipitated or adsorbed, but is a function of the C loading. Composites with low C loading show Cd sorption that is almost identical to pure Fh, while composites with high C loading show Cd sorption that is intermediate between pure Fh and pure HA, with sorption significantly enhanced over pure Fh at pH<6.5. A bidentate edge-sharing binding was identified for Cd on pure Fh and Cd-carboxyl binding on pure HA. These findings have significant implications not only for the sequestration of Cd in contaminated environments but also the coupled biogeochemical cycling of Cd, Fe and C in the critical zone.

Keywords: iron (hydr)oxides; humic acid; composites; Cd; sorption; EXAFS

1. INTRODUCTION

The geochemical cycles of iron and organic carbon (OC) are closely linked in soils and sediments. In soils iron (hydr)oxides are found coprecipitated with and coated in sorbed OC (Mikutta et al., 2014), while in marine sediments recent work estimates that ~21% of the total OC present in sediments is intimately associated with reactive iron phases (Lalonde et al., 2012). Iron−organic association may protect OC against degradation and thus promote its preservation (Mikutta et al., 2007), but the intimate association of OC with iron (hydr)oxides can also affect the crystal structure, surface properties, reductive dissolution and transformation of the iron (hydr)oxides (Schwertmann et al., 2005; Shimizu et al., 2013). It is well known that pure iron (hydr)oxides are extremely efficient sorbents of nutrients and heavy metals due to their large surface areas and abundant reactive functional groups (Schultz et al., 1987), but because of their association with OC, iron (hydr)oxide−organic composites can have significantly different reactivity towards nutrients and contaminant metals compared to their pure iron (hydr)oxide counterparts (Chen et al., 2009; Moon and Peacock, 2012; 2013; Ding et al., 2015; Wang et al., 2016). Understanding the sorption of nutrients and heavy metals with iron (hydr)oxide-organic composites is important because in natural and contaminated environments iron (hydr)oxides are typically found coprecipitated with and coated in sorbed OC (Schwertmann et al., 2005; Shimizu et al, 2013; Mikutta et al., 2014), and elemental sequestration by these iron−OC composites is a key process in the biogeochemical cycling of trace elements in the critical zone.

Ferrihydrite (Fh) is a poorly crystalline iron (hydr)oxide that is ubiquitous in geologic systems (Michel et al., 2007), occurring as the precursor to other stabilized ferric oxides such as haematite and goethite. Ferrihydrite plays a substantial role in the sequestration of trace elements in its pure and Fh–organic composite forms. Earlier reports show that 2-line Fh can sorb up to 500, 366, 250 and 62.5 mg/g Zn^{2+}, Pb^{2+}, Cd^{2+} and Cu^{2+} from aqueous solution, respectively (Rout et al, 2012). Spectroscopy evidence and modelling results indicate that trace metals such as Cu and Pb are bound to the Fh surface via inner-sphere sorption complexes (Scheinost et al., 2001; Dyer et al., 2003; Trivedi et al., 2003; Tiberg et al., 2012), Ferrihydrite–organic composites are also potent scavengers of trace metals, and often show enhanced sorption capacities compared to the isolated pure mineral end-member. For example, when Fh is coprecipitated with abiotic organic components such as fulvic acid (14.7 wt.% C), the maximum sorption capacity for Pb^{2+} is 62.7% higher (at 19.26 mg/g) and there is a higher Pb binding affinity, compared to the pure Fh (Wei et al., 2013). Similarly, when Fh is adsorbed with a simple organic ligand such as phthalate, the sorption of Cd is increased at pH 4–7 due to the formation of a surface ternary complex (Song et al., 2009). In particular however, Fh–organic composites often show enhanced sorption of metals in the mid-low pH regime compared to their pure Fh counterpart (Moon and Peacock, 2012; 2013). Work to date attributes this phenomenon to the presence of additional binding sites associated with the organic fraction and/or new high-affinity sites created when the organics adsorb to the

(hydr)oxide surfaces (Ali and Dzombak, 1996; Alcacio et al., 2001; Christl and Kretzschmar, 2001). For example, for Fh coprecipitated with biotic organic matter (OM) in the form of bacterial cells, Moon and Peacock (2012) show that Cu sorption is enhanced in the mid-low pH regime (~pH 4−5.5) compared to pure Fh, because Cu sorbs onto the bacterial fraction of the composites in addition to the mineral fraction. Furthermore, the intimate association of *Bacillus subtilis* with Fh fundamentally changes the Fh and OM physiochemical properties, compared to the isolated pure counterparts, resulting in so-called 'non-additive" sorption behaviour, where the sum of the sorptivities on the pure end-member Fh and OM does not equal the sorptivity on the Fh−OM composite. Specifically this non-additive behaviour is attributed to a surface charge effect, where in the mid-low pH regime the negative charge of the OM is reduced in the presence of the positive charge Fh, such that Cu sorption to the OM fraction of the composite is less than would be predicted according to additivity (Moon and Peacock, 2013). This non-additivity feature is also found in Cd^{2+}−ferrihydrite−*Comamonas spp* (Song et al., 2009), Pb^{2+}−ferrihydrite−*Bacillus subtilis* (Kulczycki et al., 2005), Sr^{2+}−ferrihydrite−*Shewanella alga* (Small et al., 1999) and Cu^{2+}−ferrihydrite−*Anoxybacillus flavithermu* (Franzblau et al., 2016) systems. Moreover, additivity metal sorption behaviour is also found in Cd^{2+}−kaolinite−*Bacillus subtilis* (Alessi and Fein, 2010) and Cd^{2+}−montmorillonite−*Pseudomonas putida* (Du et al, 2016b) systems. Overall the intimate association of Fh with OM, and the resulting changes in the Fh−OM

114 composite physiochemistry mean that it is difficult to predict metal sorption onto
115 Fh−OM composites in natural and contaminated environments (Moon and Peacock,
116 2013)

117 Work to date shows that careful investigation of metal sorption to Fh−OM
118 composites is essential to understand and predict both nutrient trace-metal cycling and
119 heavy-metal contamination in soils and sediments. Interaction of OM with iron
120 (hydr)oxides can occur via coprecipitation, where iron (hydr)oxide is precipitated in
121 the presence of OM, or via sorption of OM onto the iron (hydr)oxide surface (Kleber
122 et al., 2015). The physicochemical properties of these two different kinds of iron−OM
123 composites have received increasing attention recently (Eusterhues et al., 2011; Chen
124 et al., 2014; Mikutta et al., 2014), however, their environmental reactivity and
125 especially their sorption behaviour towards trace elements, still remains poorly
126 understood. Cadmium occurs naturally in the Earth's crust, and therefore is found in
127 virtually all components of terrestrial and marine ecosystems. Cadmium accumulation
128 in drinking water and food (e.g., *Oryza sativa* L.) poses severe human health issues
129 (Järup and Akesson, 2009). For example, Cd is emerging as the most serious metal
130 pollutant in China, where around 7% of total soil exceeds the environmental standard
131 limit (Du et al., 2016a).

132 In this work we investigate Cd sorption on two different kinds of Fh−OM
133 composites, namely those formed via coprecipitation with OM *versus* adsorption of
134 OM onto preformed Fh surfaces. Humic acid (HA) was chosen as a model organic

fraction to represent OM found in soils and sediments. For each composite type, coprecipitated or adsorbed, we synthesise two different composites, one with low C loading (~5 wt.% C; ~0.5 C/Fe molar ratio) and another with high C loading (~15 wt.% C; ~2 C/Fe molar ratio). We characterise the Fh−HA composites in terms of C content, specific surface area (SSA), mineralogy and crystallinity, organic C composition and fractionation and nano-scale Fe-C elemental distribution. We then combine macroscopic adsorption edge experiments with microscopic Cd K-edge EXAFS to explore the sorption behaviour of Cd from a macro- and molecular-level. Our findings help understand Fe−OM−metal interactions in soils and sediments where OM interaction with iron (hydr)oxides and drawdown of trace elements coexist.

2. MATERIALS AND METHODS

2.1 Ferrihydrite and ferrihydrite-humic acid composite preparation and characterisation

A commercial humic acid sodium salt was procured from Sigma−Aldrich (H16752−2; Shanghai, China). Purification of the solid HA was done following Du et al. (2016a). Because humic acid is soluble in alkaline condition, HA suspension was prepared by dissolving the purified HA in 0.1 M NaOH. The pH of the HA suspension was adjusted to ~7 before using. The mass fraction of carbon in the HA was determined by a Leco SC–444DR dual range sulfur and carbon analyser as ~37.8 wt.% (Table S1). 2-line ferrihydrite (Fh) was prepared via rapid hydrolysis of Fe^{3+} salt solution to pH

~7.5 with 1 M KOH (Moon and Peacock, 2012). Two different Fh−HA composites were prepared, i.e., coprecipitated Fh−HA and adsorbed Fh−HA. For the coprecipitated Fh−HA, 0.1 M Fe^{3+} salt solutions were first mixed with two different amounts of HA under vigorous stirring, generating C/Fe mass ratios of 0.1 and 0.5, which was equal to molar C/Fe ratio of 0.47 and 2.33, respectively. After 30 minutes, the pH of the suspensions was raised to 7.5 by the dropwise addition of 1 M KOH. These preparations should result in Fh−HA coprecipitated composites with approximately 5 wt.% and 15 wt.% C [assuming the structural formula for 2-line Fh of $FeOOH–0.4H_2O$ (Hiemstra and Riemsdijk, 2009)], named as FhHA_Cor5% and FhHA_Cor15%, respectively. For the adsorbed Fh−HA, two different amounts of HA were mixed with the freshly prepared Fh under vigorous stirring, generating initial C/Fe mass ratios of 0.1 and 0.5. The pH of the suspension was then adjusted to ~7.5 by the dropwise addition of 1 M KOH and the suspension was allowed to react for 4 hours. The suspensions were centrifuged at 4000 ***g*** for 20 minutes, and the supernatant was removed. As for the Fh−HA adsorption composites, these preparations should result in Fh−HA adsorption composites with approximately 5 wt.% and 15 wt.% C, named as FhHA_Adsr5% and FhHA_Adsr15%, respectively. Both the pure Fh and Fh–HA composites were washed three times with MilliQ water and dialysed for 3 days. During the washing and dialysis procedures, a small fraction of the loosely-bound HA was dissolved from the solid products (measured by colorimetric method) and this fraction of HA was removed. The freshly prepared Fh and Fh–HA

177 composites were used for metal sorption experiments while a portion of the wet
178 samples were freeze-dried for total C content, BET, XRD, carbon K-edge NEXAFS
179 and Fe K-edge XAS measurements.

180 The total carbon contents of the Fh–HA composites were determined using a
181 Leco SC–444DR dual range sulfur and carbon analyser (Leco Co. Ltd., Chicago,
182 USA). The surface area of the dried and degassed samples were measured by the BET
183 method using a Micromeritics Gemini VII analyser (Micromeritics Co. Ltd., Atlanta,
184 USA). The C contents and BET measurements were conducted in triplicate. Mineral
185 identity was determined with a Bruker D8 Advance power diffractometer (Bruker
186 AXS, Karlsruhe, Germany) and Cu Kα radiation (λ=0.16054 nm). The coprecipitates
187 and adsorption composites were also investigated using a NanoSIMS 50L (Cameca
188 Co. Ltd., Gennevilliers, France) equipped with a caesium ion probe (Cs^+) (Li et al.,
189 2017). Prior to NanoSIMS analysis, the fresh samples were immobilized on Si wafers
190 (~10 mm diameter) and left to air-dry. The primary beam (~1 pA) stepped over the
191 sample at a 256×256 pixel resolution with a lateral resolution of 100–200 nm.
192 Secondary ions of $^{12}C^-$ and $^{56}Fe^{16}O^-$ were simultaneously collected with an electronic
193 dead time fixed at 44 ns. The ImageJ software (1.44p version, National Institutes of
194 Health, USA) was used to process the images. The correlation analyses were
195 performed using JACoP, a novel plug-in of Image J.

196

197 **2.2 Cadmium sorption on ferrihydrite and ferrihydrite–humic acid composites**

198 Batch sorption edge experiments were performed in 50 mL plastic centrifuge tubes at
199 25 ºC. KNO_3 stock solution was prepared at 0.1 M for use as background electrolyte.
200 Cd stock solution was prepared at 8.90 mM from $Cd(NO_3)_2 \cdot 4H_2O$. Sorption samples
201 at 3.33 g sorbent L^{-1} and 0.4 mM $[Cd]_{total}$ were prepared by mixing 1.35 mL 8.90 mM
202 Cd stock solution with 0.1 g (dry weight) of freshly prepared ferrihydrite or
203 ferrihydrite–HA composite in 28.65 mL of 0.1 M KNO_3. At 100% sorption,
204 experiments contained ~1.35 wt.% Cd. For Cd sorption on pure HA, 1.35 mL Cd
205 stock solution was mixed with a known amount of HA suspension to achieve the same
206 sorbent (3.33 g sorbent L^{-1}) and metal concentration (0.4 mM). The pH of the
207 resulting suspensions was adjusted to ~4–8 by dropwise addition of either HNO_3 or
208 KOH. Sorption samples were then shaken continuously for 24 hours during which
209 time the pH of the suspensions was adjusted every 4 hours to hold constant at ± 0.05
210 pH units of the set pH values. Cd adsorption experiments with Fh show that 24 hours
211 is sufficient for adsorption equilibrium to occur (Tiberg and Gustafsson, 2016). The
212 final pH of the suspensions was recorded before centrifugation (4000 ***g***, 20 minutes).
213 The supernatants were then filtered through 0.22 µm membrane filters and 3k Dalton
214 ultrafilters if necessary and acidified with 1% HNO_3 for measurement of Cd by ICP–
215 MS (Thermo Fisher Scientific, Massachusetts, USA). Experimental sorption solution
216 speciation was determined by PHREEQC using the MINTEQ.V4 database (Moon and
217 Peacock, 2012). Sorption samples that separated in the bottom of the centrifuge tubes
218 (as thick pastes) were collected for Cd K-edge XAS analysis.

2.3 X-ray absorption spectroscopy

Ferrihydrite and the Fh–HA composites were characterized by Fe K-edge XAS. Fe XAS spectra were collected at Fe K-edge (~7.111 keV) in transmission model on beamline 1W1B of Beijing Synchrotron Radiation Facility (BSRF). During data collection, storage ring electron energy is 2.5 GeV and the beam current varied between 130 and 250 mA. The carbon (1s) NEXAFS spectra of pure HA and Fh–HA composites were collected at the BL08U1 beamline of the Shanghai Synchrotron Radiation Facility (SSRF, China). The storage ring energy was 3.5 GeV and the beam current varied between 150–210 mA. The sample holder contained a number of Cu windows topped with ~5 μm thickness powdered samples and was loaded into the beamline vacuum system. Carbon K-edge spectra were collected in the total electro yield (TEY) model in the energy ranges from 278 to 310 eV, during which the step size was 0.2-eV for 280–283 eV, 0.1-eV for 283–292 eV and 0.2-eV for 292–310 eV regions.

Cd XAS spectra of sorbed samples were collected in fluorescence mode on station B18 at Diamond Light Source (DLS) Ltd., UK. The storage ring energy was 3.0 GeV and the beam current varied between 130 and 240 mA. Samples were prepared as a thick paste held in a slotted Teflon holder, and covered with Kapton film, and were stored at 4 ºC to prevent drying before XAS collection. Since carboxyl ligands comprise the majority of reactive sites in humic substances below pH 7,

metal-carboxyl binding is expected to be an important mechanism for sorption of metal cations by HA (Holtzclaw and Sposito, 1979). To represent the immediate binding environment of Cd complexed to carboxyl groups, an aqueous Cd-Acetate solution was prepared at a Cd:ligand molar ratio of 1:100 by mixing equal volumes of 0.05 M $Cd(NO_3)_2$ with 5 M acetic acid (Ac) solution. The pH of the CdAc was adjusted to 3 to promote the complexation of aqueous Cd^{2+} with carboxyl groups. The solution speciation for CdAc was determined in Visual Minteq, and the percentage distribution of Cd species was 54.3% Cd-$Acetate^{+}$, 22.1% Cd-$(Acetate)_2$ and 4.863% Cd-$(Acetate)_3^{-}$.

Analyses of the C, Fe and Cd K-edge XAS data were accomplished using the IFEFFIT package (Ravel and Newville, 2005). The C NEXAFS spectra were baseline corrected and normalised in ATHENA. Background subtraction and normalisation of the Fe and Cd K-edge XAS data were carried out in ATHENA. The input parameter of R_{bkg} was set to 0.9 in the analyses of Fe and Cd XAS spectra. Fourier transforms were generated on k^3-weighted spectra over an approximate k range of 3–12 $Å^{-1}$ using Hanning windows. The theoretical Fe and Cd EXAFS models were built by using FEFF 6.0 in the IFEFFIT package. Least-squares fits of the Fourier-transformed $k^3\chi(k)$ data were determined by shell simulations using ARTEMIS.

Linear combination fitting (LCF) using ATHENA was employed to determine the partitioning of Cd between the Fh and HA fractions in the Fh–HA composites using a linear combination of the end-member Cd-Fh and Cd-Carboxyl spectra. This method

has been widely used to determine the distribution of metals in complex sorbent systems (Moon and Peacock, 2012; Du et al., 2016b; 2017). The linear combination was performed in *k* space over 3–12 $Å^{-1}$. The errors associated with the fits are those typically applied to 2-component mixtures where errors are estimated to be approximately ±10% of the fitted values (Kim et al., 2000). The goodness of the fits was characterized by the *R*-factor, where $R<0.1$ indicates a good fit.

3. RESULTS AND DISCUSSION

3.1 Physiochemical characteristics of ferrihydrite−humic acid composites

3.1.1 C contents and specific surface area

The results for the C contents and SSA of the Fh and Fh–HA composites are shown in Table S1. Coprecipitation of Fh with HA results in a higher C content (14.6±0.15 wt.%, 5.4±0.01 wt.%) than adsorption with HA (12.1±0.15 wt.%, 4.5±0.04 wt.%). This agrees with previous work studying the reaction of Fe oxides with forest floor OM (Chen et al., 2014; Mikutta et al., 2014). The SSA of the pure Fh is 310.4±2.5 m^2/g, but HA reduces the SSA of both the Fh−HA coprecipitates and adsorption composites. Specifically, at ~5 wt.% C, the SSA of the Fh−HA composites decreases to 239.3±2.8 m^2/g and 184.7±2.4 m^2/g for the adsorption and coprecipitation composites, respectively, while at ~15 wt.% C, SSA declines to 164.6±2.08 m^2/g and 0.24 m^2/g, for the adsorption and coprecipitation composites, respectively. The SSA for the ~15 wt.% C Fh−HA coprecipitated composite is similar

to the SSA of freeze-dried HA (0.17±0.01 m^2/g). Given the drastic reduction in SSA for the ~15 wt.% C coprecipitated composite, our results suggest that HA can promote the formation of N_2-inaccessible aggregates, and that this phenomenon appears to be more prevalent in Fh−HA coprecipitated composites. A similar observation is reported for Fh−OM coprecipitates in the study of Mikutta et al. (2014).

3.1.2 Mineralogy

The pure 2-line Fh shows two distinct broad peaks at ~0.15 nm and 0.26 nm (Fig. S1). The XRD patterns of FhHA_Cor5% and FhHA_Adsr5% resemble those of the 2-line Fh, whereas FhHA_Cor15% and FhHA_Adsr15% exhibit reduced crystallinity, especially for the coprecipitation composite in which the peak at ~0.26 nm disappears. This is in good agreement with previous studies of Fh−OM composites (Moon and Peacock, 2012; Chen et al., 2014; Mikutta et al., 2014). This reduced crystallinity is probably due to the frequent reactions between $Fe(O, OH)_6$ octahedra of Fh and HA molecules that may prevent cross-linking and result in decreased size of coherent scattering domains (Eusterhues et al., 2008). Broad peaks occurring in the low Bragg-angle region (~0.49 nm) likely originate from HA molecules (Eusterhues et al., 2011; Mikutta et al., 2014).

Fe EXAFS can provide information on the relative crystallinity of mineral phases by evaluating the type and number of Fe−Fe polyhedral linkages. Visual comparison of the pure Fh and Fh−HA composites show that the Fh−HA composites have a similar basic structure to pure Fh (Fig. S2a). The 5 spectra all resemble one another,

and the peak features at *k* ~5.0, ~7.5, ~9.7 and 10.4 Å are indicative of high-shell backscattering atoms. In *R* space, the first peak (~1.95 Å) corresponds to the nearest coordinated O atoms (Fig. S2b). The second shell consists of two distinct Fe−Fe coordination environments at *R* distance of ~3.0 and 3.4 Å. For pure Fh, the first shell consists of 5.11 O atoms at a Fe−O bonding distance of ~1.96 Å, while the second shell has 2.75 Fe atoms at ~3.04 Å, and 3.54 Fe atoms at ~3.43 Å (Table S2). The shorter Fe−Fe distance is normally attributed to Fe–Fe edge-sharing and the longer distance to Fe−Fe double corner-sharing configuration (Wang et al., 2016). The first shell Fe−O (~1.96−1.97 Å) and the second shell Fe−Fe distances (~3.03−3.04 Å; ~3.43−3.44 Å) for the Fh−HA composites are equivalent to those of the pure Fh. The coordination number for the Fe−Fe edge-sharing (2.70−2.71) and corner-sharing (3.37−3.50) atoms for the Fh−HA composites are smaller than those of the pure Fh. However, the errors associated with coordination number (±0.4−0.7) mean that the HA fraction does not appear to change the average local environment of Fe in the Fh−HA composites.

3.1.3 Humic acid composition

The C-NEXAFS spectra of HA and Fh−HA composites are presented in Fig. 1. For pure HA, three major bands are pronounced at ~285.1 eV, 286.8 eV and 288.4 eV, corresponding to aromatic (1 s-π*, C=C), phenolic (1 s-π*, C=C−O) and carboxylic (1 s-π*, C=O) C, respectively (Chen et al., 2016). Compared with the original HA, the peaks for carboxyl C become less intense and broader in Fh−HA composites,

signifying the interaction of these groups with the mineral surfaces, likely via ligand exchange between FeOH groups and carboxylic groups (Chen et al., 2014). For FhHA_Adsr5% and FhHA_Cor5% the aromatic C and phenolic C are strongly evident, and the alkyl C peaks at 289.6 eV increase, compared to pure HA, suggesting all fractions of the HA can be adsorbed/coprecipitated with the Fh mineral at relatively low HA surface loading. For FhHA_Adsr15% and FhHA_Cor15%, however, the aromatic C peaks are still strongly evident but the peaks for phenolic and alkyl C decline, suggesting selective uptake of the aromatic fraction of the HA at higher HA surface loading. Observations by Chen et al. (2014) showed that aromatic C is preferentially associated with Fh-OM composites at molar C/Fe ratio of 1.5 which is close to those (~C/Fe ratio of 2) of the FhHA_Adsr15% and FhHA_Cor15% products in this study. Specifically, based on their C-NEXAFS spectra, FTIR analysis and UV results, Chen et al. (2014) propose that carboxyl groups attached to the aromatic rings are preferentially adsorbed or coprecipitated with Fh leading to a preferential association of aromatic C.

3.1.4 Elemental distribution of Fe and C

The nano-scale elemental distribution of Fe and C in the Fh−HA composites was mapped by measurements of the $^{56}Fe^{16}O^-$ and $^{12}C^-$ secondary ions (Fig. 2). For the FhHA_Cor5% and FhHA_Cor15% composites, the colour-coded maps of $^{56}Fe^{16}O^-$ and $^{12}C^-$ show that there is a high degree of spatial correlation between C and Fe (Fig. 2a, b; Pearson's coefficient PC>0.94). For the FhHA_Adsr5% and FhHA_Adsr15%

composites, the degree of spatial correlation is high (Fig. 2c, d; PC=0.75 and 0.86, respectively) but several separate phases of C and Fe are observed for FhHA_Adsr5% (see the ellipses in Fig. 2c). Overall all our observations suggest that C is highly spatially correlated with Fe in both the coprecipitated and adsorbed Fh−HA composites, but C distribution is more uniform in the coprecipitated type.

3.2 Aqueous Cd sorption onto ferrihydrite and ferrihydrite−humic acid composites

The experimental solution (0.4 mM $Cd(NO_3)_2$) speciation calculations show that Cd occurs predominantly as Cd^{2+} and $CdNO_3^+$ in the experimental sorption solutions (pH 4−8, Fig. S3). No Cd hydroxides and carbonates were present in our adsorption experiments. The wt.% Cd sorbed onto Fh, HA and Fh−HA composites as a function of pH is plotted in Fig. 3. At pH<5, no Cd is sorbed on pure Fh whereas a significant amount is sorbed onto HA (>90% $[Cd]_{total}$). On Fh Cd sorption increases dramatically to almost 100% sorption as pH increases from 5 to 7. The FhHA_Cor5% and FhHA_Adsr5% composites display Cd sorption that is almost identical to the pure Fh, whereas FhHA_Cor15% and FhHA_Adsr15% display Cd sorption that is intermediate to that of the end-member Fh and HA. This macroscopic sorption behaviour implies that there is a contribution of the HA fraction to the sorption of Cd, specifically enhancing Cd sorption in the mid-low pH regime. Relatively few studies investigate metal sorption by organo-mineral composites, but enhanced sorption to iron

(hydr)oxide organo-mineral composites in the mid-low pH regime is also seen during Cd sorption to composites made with organic acids (Song et al., 2008) and bacteria (Song et al., 2009), and also during the sorption of other metals (e.g., Cu, Pb, Sr et al.,) to composites made with organic acids and bacteria (Tipping et al., 1983; Murphy et al., 1995; Ali and Dzombak, 1996; Alcacio et al., 2001; Christl and Kretzschmar, 2001; Buerge-Weirich et al., 2003; Flogeac et al., 2004; Saito et al., 2005; Jönsson et al., 2006; Zhu et al., 2010; Moon and Peacock, 2012; 2013). In these cases enhanced sorption is generally attributed to the presence of additional binding sites associated with the organic fraction and/or new high-affinity sites created when the organics adsorb to the (hydr)oxide surfaces. Furthermore, Cd sorption is approximately equivalent between the FhHA_Cor5% and FhHA_Adsr5% composites, and the FhHA_Cor15% and FhHA_Adsr15% composites. Given that the surface areas of the two 5 wt.% C composites and the two 15 wt.% C composites are significantly different (Table S1), this suggests that their Cd sorption capacities are not surface area and thus surface site limited, i.e., there are enough surface sites to sorb all the Cd at the experimental Cd concentration.

3.3 XAS of Cd sorption onto ferrihydrite and ferrihydrite−humic acid composites

Cd K-edge EXAFS of the Fh−HA composites were measured at two different pH, pH 5.5 and 8. Cd k^3-weighted EXAFS and Fourier transforms are shown in Fig. 4, and

387 the EXAFS fits are summarized in Table 1. The Cd-Carboxyl standard shows clear
388 visual differences to the Cd-sorbed Fh end-member spectrum, attributable to different
389 Cd−C vs. Cd−Fe coordination environments. In our Cd-Carboxyl standard, EXAFS
390 fits show that the Cd coordination environment consists of 6.73 O at ~2.27 Å and 0.82
391 C at 2.73 Å, which is in accord with monodentate Cd-Carboxyl complexation
392 (Boyanov et al., 2003). For Cd-sorbed Fh, Cd is coordinated with 6.15 O in the first
393 shell at a Cd−O bonding distance of 2.28 Å, and 1.92 Fe in the second shell at a
394 Cd−Fe distance of ~3.23 Å. In general, Cd might be sorbed via bidentate edge-sharing
395 or bidentate corner-sharing with $Fe(O,OH)_6$ polyhedra at iron (hydr)oxide surfaces
396 (Randall et al., 1999), where edge-sharing complexation results in a shorter Cd−Fe
397 distance (~3.3 Å) compared to corner-sharing complexation (~3.8 Å) (Randall et al.,
398 1999; Tiberg and Gustafsson, 2016). Our Cd−Fe distance suggests Cd complexation
399 via a bidentate edge-sharing complex at the experimental ~1.35 wt.% Cd loading.

400 For the Cd-sorbed Fh−HA composite spectra, we visually observe the presence
401 of both the Cd−C ~2.7 Å peak and the Cd−Fe ~3.2 Å peak in the Fourier transforms,
402 albeit decreased in amplitude compared to the Cd-Carboxyl standard and Cd-sorbed
403 Fh end-member spectra, respectively. In agreement with our macroscopic sorption
404 edge data, the presence of both the Cd−C and Cd−Fe peaks suggests that Cd is
405 partitioned to both the Fh and HA fractions in the composites. In addition with an
406 increase in pH from 5.5 to 8, there is a concomitant decrease in the ~2.7 Å peak and
407 an increase in the ~3.2 Å peak. To explore the partitioning of Cd between the Fh-HA

composite fractions we fit the Fh−HA composite spectra with a linear combination of the Cd-sorbed Fh end-member spectrum and the Cd-Carboxyl spectrum. At pH 5.5 the results yield an approximately equal distribution of Cd between the Fh and HA fractions, while at pH 8 Cd is partitioned more onto the Fh fraction, at approximately 70% Fh and 30% HA (Table 2). Subsequently in the EXAFS fits of the Fh−HA composite spectra, three paths of Cd−O, Cd−C and Cd−Fe were considered. For FhHA_Cor5wt%, Cd is coordinated with 2.04 C and 2.23 Fe at pH 5.5, and 1.43 C and 2.23 Fe at pH 8. For FhHA_Cor15wt%, Cd is coordinated with 2.12 C and 2.21 Fe at pH 5.5, and 0.3 C and 2.18 Fe at pH 8. For FhHA_Ads5wt%, Cd is surrounded by 2.26 C and 2.58 Fe at pH 5.5, and 0.28 C and 2.25 Fe at pH 8. For FhHA_Ads15wt%, Cd is surrounded by 2.19 C and 2.05 Fe at pH 5.5, and 1.09 C and 1.7 Fe at pH 8. The fact that the Cd−C and Cd−Fe bond lengths in the Fh−HA composites are, within error, nearly identical to the Cd-Carboxyl standard and Cd-Fh end-member spectra, respectively, shows that the immediate coordination environment around adsorbed Cd, and thus the molecular sorption mechanisms, are very similar between the Fh−HA composites and the isolated end-member Cd-Carboxyl and mineral phases. This is in good agreement with work on the molecular-level surface complexation mechanisms of Cu on Fh, organics and Fh−organic composites, where Cu is also sorbed by bidentate edge-sharing complexation on Fh fraction of Fh−organic composites, and by carboxyl binding on the organics fraction of Fh−organic composites (Moon and Peacock, 2012).

3.4 Implications for Cd mobility and fate in natural and contaminated environments

Our results show that for Fh−HA organo-mineral composites made via coprecipitation of Fh with HA and adsorption of HA onto preformed Fh, at low C concentration (~5 wt.% C; ~0.5 C/Fe molar ratio) total Cd sorption is not significantly different to that observed on pure Fh (Fig. 3). Sorbed Cd is however, distributed between the Fh and HA composite fractions as a function of pH (Fig. S4). At higher C concentration (~15 wt.% C; ~ 2 C/Fe molar ratio) coprecipitated and adsorbed composites display total Cd sorption that is intermediate between pure Fh and pure HA, and show significantly elevated Cd sorption in the mid-low pH regime (Fig. 3). In addition, sorbed Cd is again distributed between the Fh and HA composite fractions as a function of pH (Fig. S4). At both low and high C concentrations, our results show that for all composites sorbed Cd is distributed approximately equally between the Fh and HA fractions at low pH, and preferentially distributed on the Fh fraction at high pH (Table 2, Fig. S4). The reason why the low C composites show total Cd sorption that is no different to pure Fh, i.e., say that they are not behaving additively, is probably due to the occurrence of less carboxyl sites during the binding of the HA to the Fh surface (Karlsson and Persson, 2012), as evidenced by our C-NEXAFS results (Fig. 1). In contrast, the high C composites show total Cd sorption that is intermediate to pure Fh and pure HA, i.e., say that there is a degree of additivity in their sorption behaviour.

This might because there are more HA carboxyl sites, so even after these sites are used up in the binding of the HA to the Fh surfaces, there are still sufficient sites to complex with Cd, and this is manifest in the mid-low pH regime where carboxyl sites are negatively charged, while Fh sites are positively charged, and thus the carboxyl sites provide additional binding sites for enhanced complexation of Cd.

The fact that total sorbed Cd is a function of the C concentration in Fh-HA composites, and the fact that the distribution of sorbed Cd between the Fh and HA composite fractions is a function of pH has important implications for Cd mobility and fate in natural and contaminated environments. In the first case, our results indicate that in environments where iron (hydr)oxides are coprecipitated and adsorbed with elevated concentrations of organic substances, there will be significantly enhanced total Cd sorption to these composites in the mid-low pH regime, compared to the sorption expected for pure iron (hydr)oxides and those only minimally intermixed with organics. This has direct relevance to organic-rich soils and sediments, acid-mine drainage environments, and black water rivers, and it is therefore critical to measure and subsequently model Cd sorption to iron (hydr)oxide composites. Results here provide a molecular understanding of Cd sorption to Fh composites as a function of composite C concentration and environmental pH, which can be used to inform and constrain subsequent thermodynamic modelling studies. In the second case, despite the fact that Cd is sorbed as an inner-sphere complex to both the Fh and HA fractions, and should therefore be relatively robust to exchange or desorption (at approximately

471 constant pH), the relative mobility of the Cd sorbed to the different Fh and HA
472 fractions might differ as a function of environmental changes (e.g., during organic
473 decomposition and sediment diagenesis). In this scenario, as above, pure Fh may not
474 be a suitable analogue for predicting mobility and thus eventual fate of Cd in natural
475 and contaminated environments. Furthermore, although the chemical composition of
476 the coprecipitated HA is similar to the adsorbed HA, based on our C-1s NEXAFS
477 results, the stability of Cd-containing Fe−HA coprecipitated *vs* adsorbed composites,
478 however, could be quite different as the ability of microorganisms or microbial
479 enzymes to access internally occluded coprecipitated HA *vs* surface adsorbed HA may
480 differ. There is currently a dearth of knowledge on the stability of coprecipitated and
481 adsorbed OM during long-term biodegradation, and this should be addressed in
482 further studies. In summary, this batch and molecular sorption study shows that the
483 coprecipitation and adsorption of HA with Fh modifies the physiochemical properties
484 of the resulting Fe−HA composites, which exerts an important effect on the
485 sequestration of Cd, and likely the coupled biogeochemical cycling of Cd, Fe and C in
486 natural and contaminated environments.
487
488 **4. CONCLUSIONS**
489 Coprecipitated Fh−HA composites show similar crystal structure, carbon composition,
490 but higher C content and smaller SSA compared to the equivalent composites formed
491 by adsorption. At high carbon loading (~15 wt.% C), enhanced Cd sorption is

observed on both coprecipitated and adsorbed composites at pH<5. At low carbon loading (~5 wt.%), however, Fh−HA composites and pure Fh sorb almost equivalent Cd over pH 4−8. Cd is sorbed as a bidentate edge-sharing on the Fh fraction and a Cd-carboxyl binding on the HA. Linear combination results demonstrate that the distribution of sorbed Cd between the Fh and HA composite fractions is a function of pH and C loading. The results yield an approximately equal distribution of Cd between the Fh and HA fractions at pH 5.5, and an approximately 70% Fh and 30% HA distribution at pH 8. All the results obtained in this study have great implications for the sequestration of Cd in organic-rich natural and contaminated environments, and also shed light on the coupled biogeochemical cycling of metal, iron and organic carbon in the critical zone.

CONFLICTS OF INTEREST

There are no conflicts of interest to declare.

ACKNOWLEDGEMENTS

This work was financed by the National Natural Science Foundation of China (NSFC) (No. 41230854), the National Basic Research Program of China (973, grant No. 2015CB150504), the NSFC–Royal Society joint project (No. 41611130184), the Royal Society Newton Mobility Grant (No. IE151033), Hunan Provincial Natural Science Foundation of China (2018JJ3239) and the Science Foundation for Young

Scholars of Hunan Agricultural University (No: 17QN37). We thank Diamond Light Source Ltd. (DLS) for access to beamline B18 (SP15019), Shanghai Synchrotron Radiation Facility (SSRF, beamline BL08U1) and Beijing Synchrotron Radiation Facility (BSRF, beamline 1W1B) where access contributed to the results presented here. We acknowledge the Institute of Geology and Geophysics, Chinese Academy of Sciences for the access to NanoSIMS.

SUPPORTING INFORMATION

Table S1, basic properties of the composite; Table S2, Fe local coordination environments; Figure S1, XRD patterns of the composite; Figure S2, Fe XAS spectra; Figure S3, Cd solution speciation; Figure S4, Cd macroscopic and microscopic sorption phenomena are available.

REFERENCES

(1) Alcacio, T.E., Hesterberg, D., Chou, J.W., Martin, J.D., Beauchemin, S., Sayers, D.E., 2001. Molecular scale characteristics of Cu(II) bonding in goethite–humate complexes. Geochim. Cosmochim. Ac. 65, 1355-1366.

(2) Alessi, D.S., Fein, J.B., 2010. Cadmium adsorption to mixtures of soil components: Testing the component additivity approach. Chem. Geol. 270, 186-195.

(3) Ali, M.A., Dzombak, D.A., 1996. Effects of simple organic acids on sorption of Cu^{2+}, and Ca^{2+} on goethite. Geochim. Cosmochim. Ac. 60, 291-304.

(4) Boyanov, M.I., Kelly, S.D., Kemner, K.M., Bunker, B.A., Fein, J.B., Fowle, D.A., 2003. Adsorption of cadmium to *Bacillus subtilis* bacterial cell walls: a pH-dependent X-ray absorption fine structure spectroscopy study. Geochim. Cosmochim. Ac. 67, 3299-3311.

(5) Buerge-Weirich, D., Behra, P., Sigg, L., 2003. Adsorption of copper, nickel, and cadmium on goethite in the presence of organic ligands. Aquatic Geochem. 9, 65-85.

(6) Chen, C.L., Hu, J., Shao, D.D., Li, J.X., Wang, X.K., 2009. Adsorption behavior of multiwall carbon nanotube/iron oxide magnetic composites for Ni(II) and Sr(II). J. Hazardd Mater. 164, 923-928

(7) Chen, C., Dynes, J.J., Wang, J., Sparks, D.L., 2014. Properties of Fe-organic matter associations via coprecipitation *versus* adsorption. Environ. Sci. Technol. 48, 13751-13759.

(8) Chen, K.Y., Chen, T.Y., Chan, Y.T., Cheng, C.Y., Tzou, Y.M., Liu, Y.T., Teah, H.Y., 2016. Stabilization of natural organic matter by short-range-order iron hydroxides. Environ. Sci. Technol. 50, 12612-12620.

(9) Christl, I., Kretzschmar, R., 2001. Interaction of copper and fulvic acid at the hematite-water interface. Geochim. Cosmochim. Ac. 65, 3435-3442.

(10) Ding, C., Cheng, W., Sun, Y., Wang, X., 2015. Effects of *Bacillus subtilis* on the reduction of U(VI) by nano-Fe 0. Geochim. Cosmochim. Ac. 165, 86-107.

(11) Du, H.H., Chen, W.L., Cai, P., Rong, X.M., Chen, C.R., Huang, Q.Y., 2016a. Cadmium adsorption on bacteria–mineral mixtures: effect of naturally occurring ligands. Eur. J. Soil Sci. 67, 641-649.

(12) Du, H., Chen, W., Cai, P., Rong, X., Dai, K., Peacock, C.L., Huang, Q., 2016b. Cd(II)

555 sorption on montmorillonite-humic acid-bacteria composites. Sci. Rep. 6, 19499.

556 (13) Du, H., Qu, C., Liu, J., Chen, W., Cai, P., Shi, Z., Yu, X.Y., Huang, Q., 2017. Molecular
557 investigation on the binding of Cd(II) by the binary mixtures of montmorillonite with two
558 bacterial species. Environ. Pollut. 229, 871-878.

559 (14) Dyer, J.A., Trivedi, P., Scrivner, N.C., Sparks, D.L., 2003. Lead Sorption onto Ferrihydrite. 2.
560 Surface complexation modeling. Environ. Sci. Technol. 37, 915-922.

561 (15) Eusterhues, K., Wagner F.E., Häusler W., Hanzlik M., Knicker H., Totsch, K. U.,
562 Kögel-Knabner, I., Schwertmann, U., 2008. Characterization of ferrihydrite-soil organic
563 matter coprecipitates by X-ray diffraction and Mössbauer spectroscopy. Environ. Sci. Technol.
564 42, 7891-7897.

565 (16) Eusterhues, K., Rennert, T., Knicker, H., Kögelknabner, I., Kai, U.T., Schwertmann, U., 2011.
566 Fractionation of organic matter due to reaction with Ferrihydrite: Coprecipitation versus
567 adsorption. Environ. Sci. Technol. 45, 527-533.

568 (17) Flogeac, K., Guillon, E., Aplincourt M., 2004. Surface complexation of copper(II) on soil
569 particles: EPR and XAFS studies. Environ. Sci. Technol. 38, 3098-3103.

570 (18) Kulczycki, E., Fowle, D.A., Fortin, D., Ferris, F.G., 2005. Sorption of cadmium and lead by
571 bacteria–ferrihydrite composites. Geomicrobiol. J. 22, 299-310.

572 (19) Franzblau, R.E., Daughney, C.J., Swedlund, P.J., Weisener, C.G., Moreau, M., Johannessen,
573 B., Harmer, S.L., 2016. Cu(II) removal by *Anoxybacillus flavithermus*-iron oxide composites
574 during the addition of Fe(II)aq. Geochim. Cosmochim. Ac. 172, 139-158.

575 (20) Hiemstra, T., Riemsdijk, W.H.V., 2009. A surface structural model for ferrihydrite I: Sites

related to primary charge, molar mass, and mass density. Geochim. Cosmochim. Ac. 73, 4423-4436.

(21) Holtzclaw, K.M., Sposito, G., 1979. Analytical properties of the soluble, metal-complexing fractions in sludge-soil mixtures: IV. Determination of carboxyl groups in fulvic acid. Soil Sci. Soc. AM. J. 43, 318-323.

(22) Järup, L., Akesson, A., 2009. Current status of cadmium as an environmental health problem. Toxicol. Appl. Pharm. 238, 201-208.

(23) Jönsson, J., Sjöberg, S., Lövgren, L., 2006. Adsorption of Cu(II) to schwertmannite and goethite in presence of dissolved organic matter. Water Res. 40, 969-974.

(24) Karlsson, T., Persson, P., 2012. Complexes with aquatic organic matter suppress hydrolysis and precipitation of Fe(III). Chem. Geol. 322-323, 19-27.

(25) Kim, C.S., Brown Jr, G.E., Rytuba, J.J., 2000. Characterization and speciation of mercury-bearing mine wastes using X-ray absorption spectroscopy. Sci. Total Environ. 261, 157-168.

(26) Kleber, M., Eusterhues, K., Keiluweit, M., Mikutta, C., Mikutta, R., Nico, P.S., 2015. Mineral–organic associations: formation, properties, and relevance in Soil Environments. Adv. Agron. 130, 1-140.

(27) Lalonde, K., Mucci, A., Ouellet, A., Gélinas, Y., 2012. Preservation of organic matter in sediments promoted by iron. Nature 483, 198-200.

(28) Li, Q., Du, H., Chen, W., Hao, J., Huang, Q., Cai, P., Feng, X., 2017. Aging shapes the distribution of copper in soil aggregate size fractions. Environ. Pollut. 233, 569-576.

(29) Michel, F.M., Ehm, L., Antao, S.M., Lee, P.L., Chupas, P.J., Liu, G., Strongin, D.R., Schoonen, M.A., Phillips, B.L., Parise, J.B., 2007. The structure of ferrihydrite, a nanocrystalline material. Science 316, 1726-1729.

(30) Mikutta, R., Lorenz, D., Guggenberger, G., Haumaier, L., Freund, A., 2014. Properties and reactivity of Fe-organic matter associations formed by coprecipitation *versus* adsorption: Clues from arsenate batch adsorption. Geochim. Cosmochim. Ac. 144, 258-276.

(31) Mikutta, R., Mikutta, C., Kalbitz, K., Scheel, T., Kaiser, K., Jahn, R., 2007. Biodegradation of forest floor organic matter bound to minerals via different binding mechanisms. Geochim. Cosmochim. Ac. 71, 2569-2590.

(32) Moon, E.M., Peacock, C.L., 2012. Adsorption of Cu(II) to ferrihydrite and ferrihydrite–bacteria composites: Importance of the carboxyl group for Cu mobility in natural environments. Geochim. Cosmochim. Ac. 92, 203-219.

(33) Moon, E.M., Peacock, C.L., 2013. Modelling Cu(II) adsorption to ferrihydrite and ferrihydrite–bacteria composites: Deviation from additive adsorption in the composite sorption system. Geochim. Cosmochim. Ac. 104, 148-164.

(34) Murphy, E.M., Zachara, J.M., The role of sorbed humic substances on the distribution of organic and inorganic contaminants in groundwater. Geoderma 67, 103-124.

(35) Ravel, B., Newville, M., 2005. ATHENA, ARTEMIS , HEPHAESTUS: data analysis for X-ray absorption spectroscopy using IFEFFIT. J. Synchrotron Radiat. 12, 537-541.

(36) Randall, S.R., Sherman, D.M., Ragnarsdottir, K.V., Collins, C.R., 1999. The mechanism of cadmium surface complexation on iron oxyhydroxide minerals. Geochim. Cosmochim. Ac. 63,

618 2971-2987.

619 (37) Rout, K., Mohapatra, M., Anand, S., 2012. 2-line ferrihydrite: synthesis, characterization and
620 its adsorption behaviour for removal of Pb(II), Cd(II), Cu(II) and Zn(II) from aqueous
621 solutions. Dalton T. 41, 3302-3312.

622 (38) Saito, T., Koopal, L.K., Nagasaki, S., Tanaka, S., 2005. Analysis of copper binding in the
623 ternary system Cu^{2+}/humic ccid/goethite at neutral to acidic pH. *Environ. Sci. Technol.* 39,
624 4886-93.

625 (39) Scheinost, A.C., Abend, S., Pandya, K.I., Sparks, D.L., 2001. Kinetic controls on Cu and Pb
626 sorption by ferrihydrite. Environ. Sci. Technol. 35, 1090-1096.

627 (40) Schultz, M.F., Benjamin, M.M., Ferguson, J.F., 1987. Adsorption and desorption of metals on
628 ferrihydrite: reversibility of the reaction and sorption properties of the regenerated solid.
629 Environ. Sci. Technol. 21, 863-869.

630 (41) Schwertmann, U., Wagner, F., Knicker, H., 2005. Ferrihydrite-humic associations: magnetic
631 hyperfine interactions. Soil Sci. Soc. AM. J. 69, 1009-1015.

632 (42) Shimizu, M., Zhou, J., Schroder, C., Obst, M., Kappler, A., Borch, T., 2013. Dissimilatory
633 reduction and transformation of ferrihydrite-humic acid coprecipitates. Environ. Sci. Technol.
634 47, 13375-13384.

635 (43) Small, T.D., Warren, L.A., Roden, E.E., Ferris, F.G., 1999. Sorption of strontium by bacteria,
636 Fe(III) oxide, and bacteria−Fe(III) oxide composites. Environ. Sci. Technol. 33, 4465-4470.

637 (44) Song, Y., Swedlund P.J., Singhal N., 2008. Copper(II) and cadmium(II) sorption onto
638 ferrihydrite in the presence of phthalic acid: Some properties of the ternary complex. Environ.

639 Sci. Technol. 42, 4008-4013.

640 (45) Song, Y.T., Swedlund, P.J., Singhal, N., Swift, S., 2009. Cadmium(II) speciation in complex
641 aquatic systems: a study with ferrihydrite, bacteria, and an organic ligand. Environ. Sci.
642 Technol. 43, 7430-7436.

643 (46) Tiberg, C., Sjöstedt, C., Persson, I., Gustafsson, J.P., 2012. Phosphate effects on copper(II)
644 and lead(II) sorption to ferrihydrite. Geochim. Cosmochim. Ac. 120, 140-157.

645 (47) Tiberg, C., Gustafsson, J.P., 2016. Phosphate effects on cadmium(II) sorption to ferrihydrite.
646 J. Colloid Interf. Sci. 471, 103-111.

647 (48) Tipping, E., Griffith, J.R., Hilton, J., 1983. The effect of adsorbed humic substances on the
648 uptake of copper(II) by goethite. J. Croat. Chem. Ac. 56, 613-621.

649 (49) Trivedi, P., Dyer, J.A., Sparks, D.L., 2003. Lead sorption onto ferrihydrite. 1. A macroscopic
650 and spectroscopic assessment. Environ. Sci. Technol. 37, 908-914.

651 (50) Wang, Y., Michel, F.M., Choi, Y., Eng, P.J., Levard, C., Siebner, H., Gu, B., Bargar, J.R., Jr,
652 Brown Jr, G.E., 2016. Pb, Cu, and Zn distributions at humic acid-coated metal-oxide surfaces.
653 Geochim. Cosmochim. Ac. 188, 407-423.

654 (51) Wang, X., Zhu, M., Koopal, L.K., Li, W., Xu, W., Liu, F., Zhang, J., Liu, Q., Feng, X., Sparks,
655 D.L., 2016. Effects of crystallite size on the structure and magnetism of ferrihydrite. Environ
656 Sci-Nano 3, 190-202.

657 (52) Wei, S., Xiang, W., 2013. Adsorption removal of Pb(II) from aqueous solution by fulvic
658 acid-coated ferrihydrite. J. Food Agric. Environ. 11, 1376-1380.

659 (53) Zhu, J., Pigna, M., Cozzolino, V., Caporale, A.G., Violante, A., 2010. Competitive sorption of

660 copper(II), chromium(III) and lead(II) on ferrihydrite and two organomineral complexes.
661 Geoderma 159, 409-416.

662

663

664 **Table 1. EXAFS fits of Cd local coordination environment in Cd-loaded samples.**

665

	Path	CN	R (Å)	σ^2 (10^{-3} Å^2)	ΔE_0	R-*fact* (%)
Cd-Carboxyl	Cd–O	6.73 (0.56)	2.27 (0.00)	10.5	5.6	1.8
	Cd–C	0.82 (0.23)	2.73 (0.09)	15.2		
Cd-Ferrihydrite	Cd–O	6.15 (0.55)	2.28 (0.01)	12.2	6.3	2.2
	Cd–Fe	1.92 (0.61)	3.23 (0.02)	11.9		
FhHA_Cor5% pH 8	Cd–O	7.23 (1.19)	2.27 (0.01)	14.4	3.7	1.0
	Cd–C	1.43 (0.33)	2.73 (0.12)	21.3		
	Cd–Fe	2.23 (0.31)	3.25 (0.03)	18.4		
FhHA_Cor5% pH 5.5	Cd–O	7.21 (0.61)	2.28 (0.01)	11.7	6.6	1.2
	Cd–C	2.04 (0.23)	2.76 (0.04)	7.1		
	Cd–Fe	2.23 (0.18)	3.28 (0.05)	13.0		
FhHA_Cor15% pH 8	Cd–O	6.72 (0.46)	2.28 (0.01)	13.1	5.3	0.9
	Cd–C	0.30 (0.07)	2.77 (0.03)	20.4		
	Cd–Fe	2.18 (0.20)	3.24 (0.03)	19.2		
FhHA_Cor15% pH 5.5	Cd–O	6.34 (0.62)	2.28 (0.01)	11.5	6.1	1.4
	Cd–C	2.12 (0.23)	2.77 (0.07)	20.4		
	Cd–Fe	2.21(0.14)	3.27 (0.04)	24.6		
FhHA_Adsr5% pH 8	Cd–O	6.52 (0.55)	2.27 (0.01)	12.2	5.1	1.2
	Cd–C	0.28 (0.05)	2.76 (0.01)	15.0		
	Cd–Fe	2.25 (0.62)	3.21 (0.03)	17.7		
FhHA_Adsr5% pH 5.5	Cd–O	6.61 (0.71)	2.28 (0.01)	11.3	6.0	1.8
	Cd–C	2.26 (0.32)	2.77 (0.07)	14.4		
	Cd–Fe	2.58 (0.62)	3.30 (0.04)	20.1		
FhHA_Adsr15% pH 8	Cd–O	6.51 (0.60)	2.28 (0.01)	12.5	5.0	0.9
	Cd–C	1.09 (0.12)	2.73 (0.11)	18.8		
	Cd–Fe	1.97 (0.15)	3.24 (0.03)	11.9		
FhHA_Adsr15% pH 5.5	Cd–O	6.63 (0.60)	2.28 (0.01)	10.5	6.3	1.6
	Cd–C	2.19 (0.22)	2.73 (0.05)	12.8		
	Cd–Fe	2.05 (0.35)	3.26 (0.03)	18.2		

666 CN – Coordination number, R – Inter-atomic distance, σ^2 – Debye-Wall factor, ΔE_0 – edge shift,
667 R-factor – The goodness of fit. The values of ΔE_0 for the first and second shell were set the same.

668

669

670

671

672

673

674

675

Table 2. Summary of the distribution of Cd between the ferrihydrite (Fh) and humic acid (HA) fractions (%) determined by linear combination fitting of the end-member Cd-Fh and Cd-Carboxyl EXAFS spectra.

	Distribution of Cd between the ferrihydrite (Fh) and HA fractions (%)			
pH	FhHA_Cor5%	FhHA_Cor15%	FhHA_Adsr5%	FhHA_Adsr15%
5.5	42±4 Fh, 58±6 HA	53±5 Fh, 47±5 HA	46±5 Fh, 54±5 HA	49±5 Fh, 51±5 HA
8	74±7 Fh, 26±3 HA	69±7 Fh, 31±3 HA	67±7 Fh, 33±3 HA	62±6 Fh, 38±4 HA

FIGURE CAPTIONS

Figure 1. C 1s NEXAFS spectra of the humic acid and ferrihydrite–humic acid composites.

Figure 2. $^{56}Fe^{16}O$ and $^{12}C^{-}$ secondary ion distributions in ferrihydrite–humic acid composites: a) FhHA_Cor5%, b) FhHA_Cor15%, c) FhHA_Adsr5% and d) FhHA_Adsr15%. Different colours represent different intensities of the signal, which increase from black to red. Scale bar is 5 µm. PC is the correlations between $^{56}Fe^{16}O$ and ^{12}C distribution.

Figure 3. Cd adsorption on ferrihydrite, humic acid and ferrihydrite–humic acid coprecipitated (FhHA_Cor5%, FhHA_Cor15%) and adsorbed (FhHA_Ads5%, FhHA_Ads15%) composites as a function of pH (4–8). Experimental conditions are 0.4 mM $[Cd]_{total}$ in 3.33 g sorbent L^{-1} in 0.1 M KNO_3 background electrolyte.

Figure 4. Cd k^3-weighted (a) and Fourier Transform magnitude (b) of Cd-sorbed acetate solution standard, Cd-sorbed ferrihydrite (Fh) and ferrihydrite–humic acid composites (FhHA) at different pH. The solid lines are data and dashed lines are EXAFS fits.

701 **FIG. 1**

702

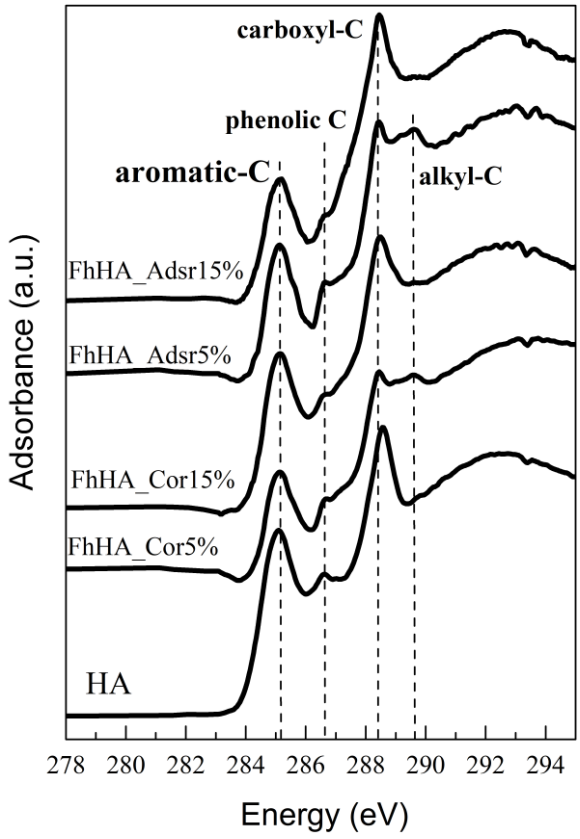

703

704 **FIG. 2**

705

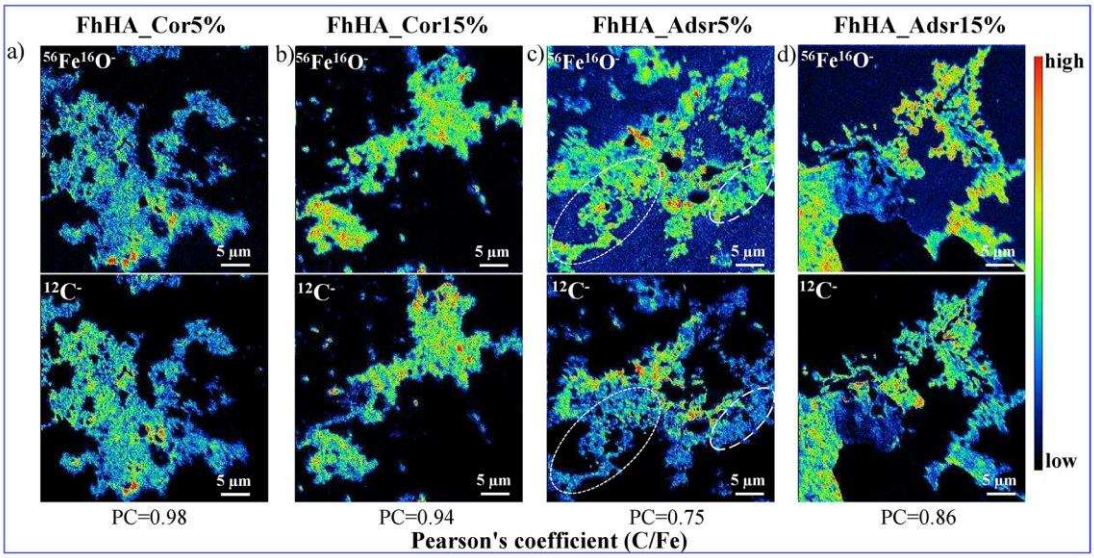

706

707

FIG. 3

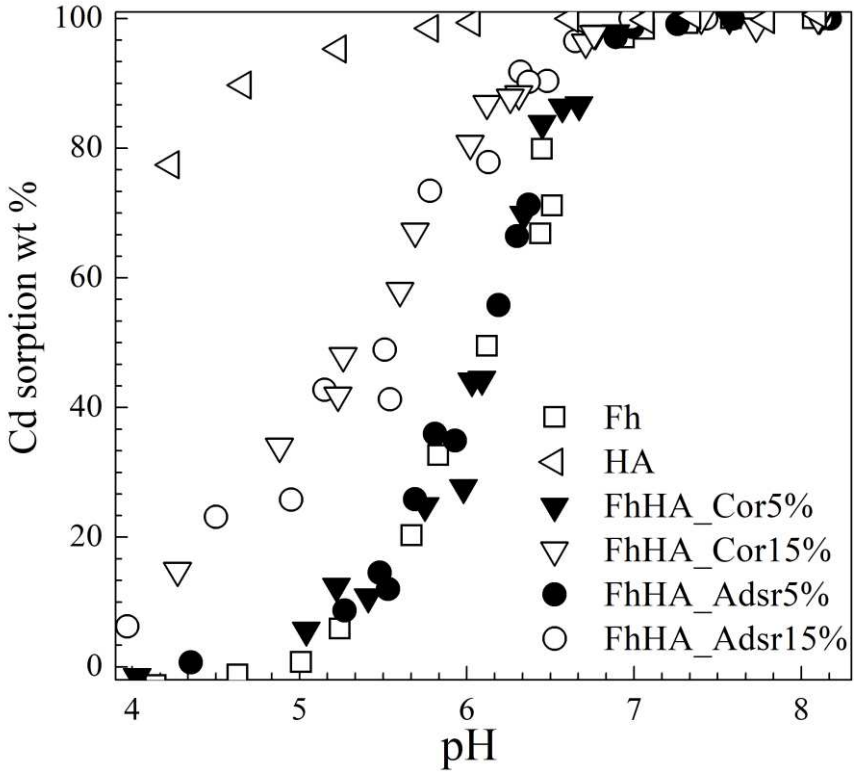
Cd sorption wt %
pH
100
80
60
40
20
0
4
5
6
7
8
Fh
HA
FhHA_Cor5%
FhHA_Cor15%
FhHA_Adsr5%
FhHA_Adsr15%

715 **FIG. 4**

716

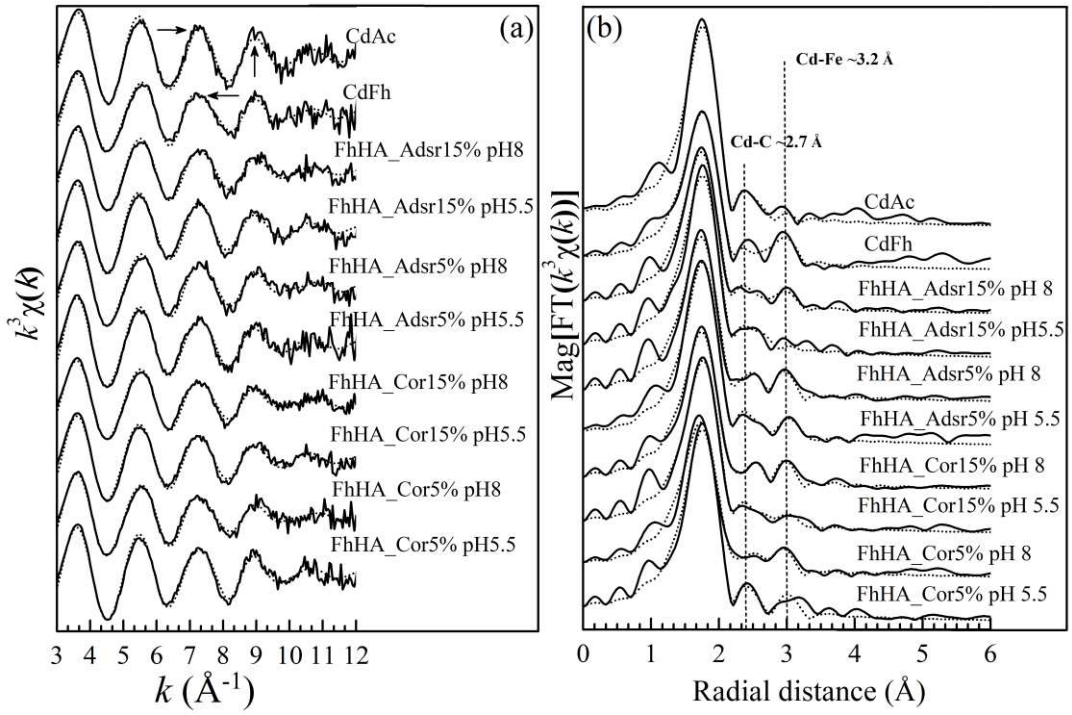

717

718

719

720

TOC Abstract